Catalysis Today 426 (2024) 114374

Contents lists available at ScienceDirect

Catalysis Today

journal homepage: www.elsevier.com/locate/cattod

5-Methoxymethyl furfural production by acid heterogeneous catalytic etherification of 5-hydroxymethyl furfural

P. Díaz-Maizkurrena [a,*], J.M. Requies [a], A. Iriondo [a], P.L. Arias [a], R. Mariscal [b]

[a] School of Engineering (UPV/EHU), Plaza Ingeniero Torres Quevedo 1, 48013, Bilbao, Spain
[b] Group of Sustainable Energy and Chemistry (EQS), Institute of Catalysis and Petrochemistry (ICP-CSIC), C/Marie Curie 2, Campus de Cantoblanco, 28049 Madrid, Spain

ARTICLE INFO

Keywords:
HMF
MMF
Zeolites
Non-noble metals
Brønsted acid sites
Lewis acid sites

ABSTRACT

The use of non-edible raw materials from agriculture as a form of biomass to obtain carbon-based compounds is the most viable solution to replace fossil resources. Within this, 5-hydroxymethyl furfural (HMF) is a platform monomer from which other high value-added monomers are obtained, such as 2,5-furandicarboxylic acid (FDCA), a compound that can be obtained from 5-methoxymethyl furfural (MMF), and which can be used as a fuel, fuel additive or polymer precursor. Several catalysts (mostly zeolites) have been tested to produce MMF. Specifically, with a ZSM-5 zeolite a yield towards this compound of 97 % has been achieved, carrying out the reaction in a batch reactor for 5 h. Through the characterization of the catalysts, a strong correlation has been observed between the acidity of these catalysts and their effectiveness in the reaction of HMF through MMF.

1. Introduction

Looking for the global trends in material extraction, from 1970 to 2017, annual global extraction of materials grew from 27.1 billion tons to 92.1 billion tons, an annual average growth of 2.6 per cent [1,2]. Within this frame of reference, fossil fuel global extraction decreased from 23 per cent in 1970 to 16 per cent in 2017 [1]. Among the issues associated with exploiting fossil resources, three could be highlighted: availability, unequal geological distribution and contribution to climate change [3,4]. The European Green Deal, presented in 2019, exposes the EU's efforts to achieve a more circular and sustainable economy, leaving aside the linear 'take-make-dispose' model [5,6]. These are compelling reasons to look for alternative ways to obtain comparable products to those obtained from fossil resources. Within this paradigm, it is pointed out in the Chemicals Strategy for Sustainability that biomass is a clear candidate as a source for obtaining bio-derived high value-added chemicals [6,7], among other types of products, such as biofuels and bioenergy.

Agricultural non-edible raw materials such as starch, cellulose and inulin [8] are renewable, inexpensive and verified starting materials for manufacturing glucose and fructose. These last C6 monosaccharides, together with C5 monosaccharides, can also be obtained from residual lignocellulosic biomass, which can reduce the problems associated with generation and management of residues. Hexoses, glucose and fructose, have been long studied and proved, especially fructose, to be a great feedstock for producing 5-hydroxymethyl furfural (HMF) [9].

Firstly discovered in the 19th century [10], HMF, whose development timeline was reviewed by Teong S.P, Yi G and Zhang Y [11], is listed within the 'Top 10 + 4' bio-based building blocks [12,13], meaning that HMF is an important platform molecule that bonds biomass, specifically carbohydrates, with fuel and chemical precursors. One of these mentioned precursors is 2,5-furandicarboxylic acid (FDCA), a monomer that can be a green alternative for the production of polymeric products. FDCA can substitute purified terephthalic acid (PTA) which is used for the production of polyethylene terephthalate (PET). The polymer that can be obtained from FDCA is called polyethylene furanoate (PEF) [14,15] and it is a green organic alternative to petroleum-based PET.

In this context, the monomer under study, 5-methoxymethyl furfural (or 5-(methoxymethyl)− 2-furaldehyde, MMF), is framed. The interest set in MMF, as one of the starting substrates for the industrial production of FDCA, must be attributed to its better storage stability than HMF [16–19] if the purpose is to storage raw material before the use in an industrial process. It means, the HMF presents storage instability, hindering the industrial FDCA production at low-cost [18]. Moreover, MMF can be obtained either directly from fructose via dehydration or from

* Corresponding author.
E-mail address: paula.diaz@ehu.eus (P. Díaz-Maizkurrena).

https://doi.org/10.1016/j.cattod.2023.114374
Received 3 February 2023; Received in revised form 19 July 2023; Accepted 10 September 2023
Available online 12 September 2023

HMF via etherification (see Fig. 1), both in methanol presence [16,20].

On the other hand, MMF itself could assume an important role as a fuel candidate and as fuel additive [17,21]. However, within the alkoxymethyl furfurals (AMFs), the 5-ethoxymethyl furfural (EMF) is the most investigated in the past.

Based on this background, the focus of this study is the MMF production though HMF/via etherification with methanol, aiming to compare the activity and selectivity of different catalysts, mainly zeolites. In this work, not only the production of MMF has been studied, but also how it is influenced by the strength and nature of the Brønsted and Lewis acid centers, and how the incorporation of non-noble metals affect the production of MMF due to the modification of the nature and strength of the acid centers. For that purpose, the catalysts were tested in batch reactor system and characterized to correlate their catalytic performance with their physicochemical properties. Afterward, non-noble metal containing catalysts were prepared using, as support, the catalyst with the best performance in the etherification reaction. These prepared catalysts were also tested, under the same operating conditions, and then characterized using the same techniques.

2. Experimental section

2.1. Materials

Synthetic 5-hydroxymethyl furfural, HMF (Sigma-Aldrich, ≥ 99.0 %) was used as standard, for chromatography analysis, and as reactant, in the chemical reaction. 5-methoxymethyl furfural, MMF (Fluorochem Ltd, 95.0 %) was used as a standard.

Anhydrous methanol, MeOH (Sigma-Aldrich, 99.8 %) was employed as reaction medium and reagent.

Zeolite Socony Mobil-5 (ZSM-5): CBV2314 with Si/Al mole ratio of 11.5 (commercialized as SiO_2/Al_2O_3 mole ratio = 23), CBV5524G with Si/Al mole ratio of 25 (commercialized as SiO_2/Al_2O_3 mole ratio = 50), CBV8014 with Si/Al mole ratio of 40 (commercialized as SiO_2/Al_2O_3 mole ratio = 80); and β zeolite CP814E with Si/Al mole ratio of 12.5 (commercialized as SiO_2/Al_2O_3 mole ratio = 25), were purchased from Zeolyst International and employed as catalysts.

Another β zeolite with Si/Al mole ratio of 12.5 (commercialized as SiO_2/Al_2O_3 mole ratio = 25), Y zeolite with Si/Al mole ratio of 2.5 (commercialized as SiO_2/Al_2O_3 mole ratio = 5), Mobil Composition of Matter No. 41 (MCM-41) with Si/Al commercial mole ratio of 5 and MCM-41with Si/Al commercial mole ratio of 10, were obtained from ACS Material, LLC and they were also used as catalysts.

Cobalt (II) nitrate hexa-hydrate ($Co(NO_3)_2{\cdot}6\,H_2O$, 98.0–102.0 %) and manganese (II) nitrate tetra-hydrate ($Mn(NO_3)_2{\cdot}4\,H_2O$, 98 %) were provided by Alfa Aesar and, copper (II) nitrate tri-hydrate ($Cu(NO_3)_2{\cdot}3\,H_2O$, 99.0–104.0 %) was acquired from Sigma-Aldrich. All of these compounds were used as metal precursors.

2.2. Catalysts preparation

The ZSM-5 zeolites were purchased on their ammonia (NH_4) form thus, to achieve the protonated form (HZSM-5), they were calcined in static air at 550 °C for 3 h. β zeolites and Y zeolites were treated the same way. Finally, MCM-41 materials were tested on their commercial form. For now on, the nomenclature used to name the different catalysts is the following: material_Si/Al, where material stands for the protonated zeolite or the MCM-41, and Si/Al is the ratio value between these elements.

The metal containing catalysts were prepared by wet-impregnation [22], incorporating approximately a 3 wt% of metal loading on the selected support. Only HZSM-5_11.5 zeolite was used as parent zeolite for this purpose and, $Co(NO_3)_2{\cdot}6\,H_2O$, $Cu(NO_3)_2{\cdot}3\,H_2O$, and $Mn(NO_3)_2{\cdot}4\,H_2O$ were employed as metal precursors to prepare these catalysts. For this impregnation process, the calculated mass of metal precursor was mixed with 1 g of the parent zeolite and 10 mL of MiliQ water in a 50 mL flask. This flask was stirred at 70 °C in a water bath for 1 h and, then, the temperature was raised up to 80 °C and vacuum was used to evaporate most of the water. After this, the flask was placed, overnight, in an oven at 100 °C, to ensure the mixture was completely dry. As a final point, the obtained powder was transferred into a refractory vessel and placed in an oven where it was reduced at 540 °C for 2 h under a 10 mL/min H_2 atmosphere, using a ramp of 5 °C/min. Nomenclature of these prepared catalysts will be M/material_Si/Al, where M ascribes the metal specie added to the support. Nomenclature is summarized in Table 1.

2.3. Characterization techniques

2.3.1. Textural properties

The Brunauer-Emmet-Teller (BET) surface area and pore characteristics of the catalysts were estimated from the N_2 adsorption-desorption isotherms obtained at − 198 °C over the whole range of relative pressure. For this characterization an Autosorb®− 1-C/TCD (Quantachrome, USA) was the equipment employed. The sample was analyzed after outgassing at 500 °C for 6 h.

2.3.2. Temperature-programmed desorption of ammonia (TPD-NH_3)

The catalysts total acidity was measured by ammonia desorption using an AutoChem II Instrument (Micrometrics, USA) equipped with a TCD detector. Firstly, the sample was heated up to 500 °C, holding this temperature for 1 h, then the temperature was cooled to 100 °C and, at this point, NH_3 (10 % v/v of NH_3 diluted in He) was fed to the sample for 30 min. The physisorbed NH_3 was removed with He for 30 min. Finally, the chemisorbed NH_3 was detected by the TCD, heating the sample to 700 °C at a rate of 10 °C/min and recording data every 1.0 s

2.3.3. Fourier-transform infrared spectroscopy (FTIR)

2.3.3.1. Py-FTIR. The density of Brønsted and Lewis acid sites (BAS and LAS) was determined by analyzing the 1400–1700 cm^{-1} wave region in the FTIR spectrum, using pyridine (Py, 99.5 %, Scharlau) as probe molecule, at 150 °C. The measurements were performed on a Nicolet 6700 FTIR spectrometer (Thermo Fisher Scientific, USA), using a Specac catalytic chamber on-line connected to it. Brønsted/Lewis acid site ratio (BAS/LAS) was quantified from the ratio between the intensity of pyridine adsorption bands at 1545 and 1450 cm^{-1}, respectively, and bearing in mind the molar extinction coefficients proposed by Emeis for both adsorption bands (ε_B = 1.67 cm/μmol) and (ε_L = 2.22 cm/μmol) [23].

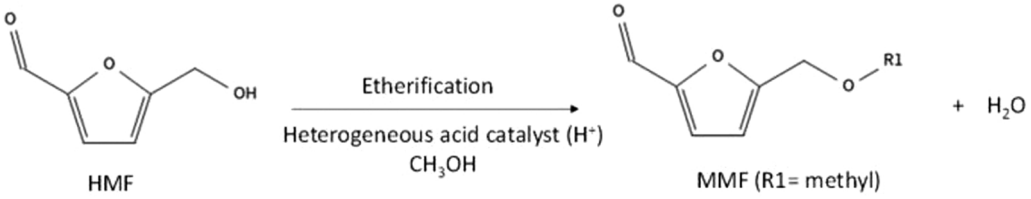

Fig. 1. Simplified reaction mechanism of HMF etherification to MMF.

Table 1
Chemical composition and textural properties of the catalysts used in HMF etherification.

Nomenclature	Commercial name	Si/Al ratio	Added metal composition %	S_{BET} $m^2 \cdot g^{-1}$	V_{micro} $cm^3 \cdot g^{-1}$	V_{meso} $cm^3 \cdot g^{-1}$	Average pore diameter nm
HZSM-5_11.5	CBV2314	11.5	-	298.90	0.123	0.092	2.96
HZSM-5_25	CBV5524G	25	-	368.30	0.100	0.351	3.82
HZSM-5_40	CBV8014	40	-	295.20	0.114	0.089	1.70
Hβ1_12.5	CP814E	12.5	-	607.10	0.203	1.151	8.69
Hβ2_12.5	Hβ	12.5	-	324.50	0.162	0.311	5.18
HY_2.5	HY	2.5	-	328.10	0.281	0.080	3.43
MCM-41_5	MCM-41	5	-	549.54	0.000	1.674	12.19
MCM-41_10	MCM-41	10	-	588.66	0.000	2.363	18.58
Co/HZSM-5_11.5	–	11.5	2.89	271.00	0.116	0.072	2.66
Cu/HZSM-5_11.5	–	11.5	2.92	288.00	0.123	0.082	2.61
Mn/HZSM-5_11.5	–	11.5	2.87	301.80	0.133	0.079	2.70

2.3.3.2. CD_3CN-DRIFT. Deuterated acetonitrile (CD_3CN, 99.8 atom % D, Sigma-Aldrich) was used as probe molecule to assess the nature and strength of the surface acid sites. CD_3CN diffuse reflectance infrared Fourier transform (DRIFT) spectra were collected with a Nicolet 5700 spectrometer equipped with an Hg–Cd–Te cryodetector with high sensitivity and working in the spectral range of 4000–650 cm^{-1}. A diffuse reflectance accessory (Praying Mantis-Harrick Co) was used as an optical mirror accessory. Samples were placed in a high-temperature catalytic reaction chamber (HVC-DRP Harrick Scientific Products, USA) that allows treatment in situ at high temperatures. Before introducing the probe molecule, the solid sample was treated at 200 °C for 1 h under an argon flow (50 mL/min) to clean the surface and cooled to 25 °C. Then, the probe molecule was added sufficiently to saturate the sample. The CD_3CN physisorbed fraction was removed by flushing with Ar flow at 100 °C for 10 min. All spectra of the deuterated acetonitrile were recorded with 128 scans accumulation and a resolution of 4 cm^{-1}.

2.3.4. Inductively coupled plasma-optical emission spectroscopy (ICP-OES)

The metal content of the catalysts was measured by ICP-OES on an Optima 2000 DV (PerkinElmer, USA) device. Prior to analyses, a 0.05 g of the samples were digested at 180 °C for 30 min in a mixture of 2 mL HCl, 3 mL HNO_3, and 3 mL HF using an ETHOS 1 Advanced Microwave Digestion System (Milestone S.r.l., Italy).

2.3.5. X-ray photoelectron spectroscopy (XPS)

A Physical Electronics PHI5700 spectrometer with non-monochromatic Mg Kα radiation (300 W, 15 kV and 1253.6 eV) with a multichannel detector was used to determinate the X-ray photoelectron spectra of the samples. These spectra were recorded in the constant pass energy mode at 39.35 eV using a 720 μm diameter analysis area. Charge referencing was measured against adventitious carbon (C 1 s at 284.8 eV).

2.4. Activity test

Regarding the experimental conditions, the employed pressure was established taking into account the literature [24], being the selected value 20 bar of N_2. In the case of the reaction temperature, a catalytic screening of reactions was carried out increasing temperature from 120 °C to 220 °C with a step of 20 °C, finally chosen a temperature of 160 °C. In this way, the pressure and the temperature played part of fixed conditions, taking the reaction time as variable condition. The catalytic tests were carried out for 1 and 3 h of reaction time. After that, those catalysts with the best catalytic were also tested for 5 and 10 h of reaction time.

All reactions were carried out in a 50 mL (± 5 mL) batch-type Teflon-lined stainless-steel autoclave lined with a 30 mL (± 5 mL) glass vessel (Iberfluid instruments, S.A. and Kalrez Spectrum). The production of MMF from HMF was carried out using 15 g solution of HMF/MeOH (1/99 wt ratio) and 0.05 g of the selected catalyst [24]. After loading this mixture in the reactor, it was sealed and pressurized by 20 bar of N_2 and then placed in a heated plate with 500 rpm magnetic stirring. Once the reaction time has been completed, the autoclave was cooled down by placing it in an ice bath to ensure the end of the reaction, then, the pressure was released. The liquid product obtained was filtered and then analyzed by a high-performance liquid chromatograph (HPLC 1260 Infinity equipped with a Hi-Plex H column and infrared detector, Agilent Technologies, USA) using MiliQ water as mobile phase. This same equipment was used to determine the amount of HMF fed. The quantification was carried out using the external standard method. An internal pattern, specifically 3 wt% isoProOH in MiliQ water, was employed, to ensure the optimal performance of the device.

Catalytic activity results are expressed as conversion of HMF and yield of MMF, which are calculated by the following equations:

$$Conversion \quad (\%) = \frac{N^{in}_{HMF} - N^{out}_{HMF}}{N^{in}_{HMF}} \cdot 100 \tag{1}$$

$$Yield \quad (\%) = \frac{N^{out}_{MMF}}{N^{in}_{HMF}} \cdot 100 \tag{2}$$

being N, moles of each compound.

Additionally, gas chromatography/mass spectrometry (GC/MS-QP2010 SE Shimadzu, Agilent Technologies, USA; equipped with a TRB-WAX column, Teknokroma Analitica SA, Spain) analyses were also conducted to evaluate qualitatively the possible secondary products.

3. Results and discussion

3.1. Catalysts characterization

3.1.1. Chemical composition and textural properties

The nomenclature used for easier identification of samples, the chemical composition determined by ICP-OES and the textural properties obtained from N_2 adsorption-desorption isotherms for outgassed samples are given in Table 1. Data associated with chemical composition showed that metal loading achieved by wet-impregnation method was near to the nominal one.

Regarding textural properties, the BET surface area (S_{BET}), the microporous volume (V_{micro}) obtained by the t-method (Boer, Linden, van der Plas and Zondervan), the mesoporous volume (V_{meso}) which was calculated using the BJH method (Barrett, Joyner and Halenda) and the average pore diameter are the parameters presented in Table 1.

The HZSM-5_11.5 and HZSM-5_40 catalysts show similar porosity properties, being only the average pore volume slightly higher in the case of HZSM-5_11.5. The HZSM-5_25 catalyst registers the highest S_{BET} of the HZSM-5 type catalysts, as well as the highest mesoporous volume, in contrast with the lowest microporous volume, and the highest average pore diameter. Summing this up, it could be said that HZSM-5_25 possesses higher pore volume due to its pores are bigger than its HZSM-5 counterpart's, resulting in higher BET surface area.

The Hβ1_12.5 catalyst shows a value of BET surface area of 607 m^2/g, almost twice the one of the HZSM-5 catalysts, having also higher

mesoporous volume. This observation seems to be in accordance with the results reported in the literature [25]. In the case of the Hβ2_12.5 zeolite, its pore structure presents lower S_{BET} than the Hβ1_12.5 catalyst, similar to the one of the HY_2.5 zeolite and HZSM-5_25. Unless the HY_2.5 zeolite has similar BET surface area to the Hβ2_11.5 one, its average pore diameter and mesoporous volume are lower, being higher the proportion of micropores and being this proportion of microporous volume similar to Hβ1_11.5.

The MCM-41 catalysts show surface area, pore volume and average pore diameter above 500 m^2/g, 1.7 cm^3/g, and 12 nm, respectively. These data mean that these catalysts have the largest pore size and, therefore, the most mesoporous structure of catalysts screened, since they do not present microporous contribution as can be seen in Table 1. This fact is concordance with bibliography [26].

As aforementioned, the HZSM-5_11.5 catalyst has also been employed as support to prepare the monometallic catalysts indicated on the last three lines of Table 1. According to these data, the incorporation of cobalt or copper into the support has reduced the parameters presented in the table. This fact indicates that metals were deposited preferentially within the porous structure. A similar phenomenon is observed for the Mn monometallic catalyst. However, it shows slightly higher S_{BET} than the no-loaded HZSM-5_11.5, suggesting that superficial exposure of Mn particles is better than the superficial exposure on supported Co and Cu catalysts [27].

3.1.2. Temperature-programmed desorption of ammonia

The acidity properties of the tested catalysts were measured by two complementary techniques, the temperature-programmed desorption of ammonia (NH_3-TPD) and the infrared Fourier spectroscopy (FTIR). These mentioned techniques are commonly employed for zeolite characterization [28]. Since NH_3-TPD only provides information on total acidity and acid strength distribution of solid catalytic materials [29], the Py-FTIR and CD_3CN-DRIFT techniques were used to differentiate the Brønsted and Lewis acid sites and their strength, respectively.

Profiles obtained with NH_3-TPD technique are shown in Fig. 2 and Fig. 3, while the derived data, associated with distribution of acid sites and total amount of acid sites, are shown in Table 2. The profiles of the catalyst without metal load are shown in Fig. 2 and they can be classified in three well-defined shapes. One of these shapes belongs to the HZSM-5 type zeolites. The second one belongs to the Hβ zeolites, and the HY zeolite. The third one is the one related to the MCM-41 materials.

Regarding the HZSM-5 catalysts, their ammonia desorption profiles show two desorption peaks at, around, 195–230 °C and 400–440 °C, indicating that these catalysts have centers with different acid strength. According to literature [26,30–35], the peaks that appear at low temperatures can be ascribed to weak and/or medium bonded ammonia desorption. While the peaks at higher temperatures are associated with desorption of ammonia strongly interacting with acid sites.

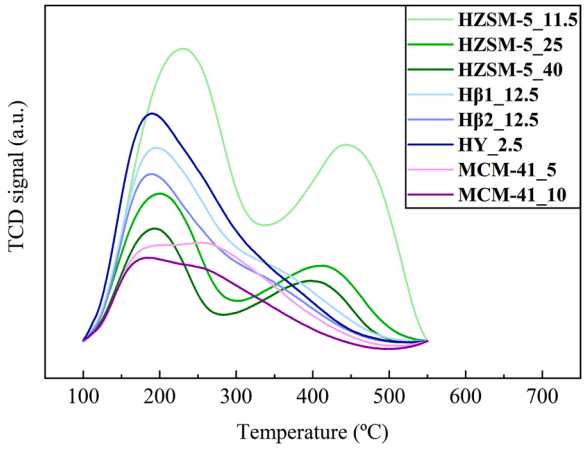

Fig. 2. NH_3-TPD for tested catalysts (without metal).

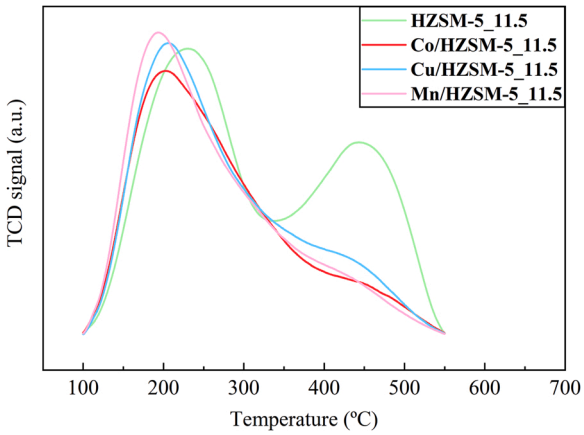

Fig. 3. NH_3-TPD for HZSM-5_11.5 and non-noble metal impregnated HZSM-5_11.5.

Table 2
Data obtained from deconvolution of NH_3-TPD profiles for all of the tested catalysts.

Sample	Distribution of acid sites				Total amount of acid sites (mmol $NH_3 \cdot g_{cat}^{-1}$)
	Weak-medium		Strong		
	T_{max} (°C)	mmol $NH_3 \cdot g_{cat}^{-1}$	T_{max} (°C)	mmol $NH_3 \cdot g_{cat}^{-1}$	from 100° to 550°C
HZSM-5_11.5	230	1.538	440	1.155	2.693
HZSM-5_25	200	0.550	420	0.420	0.969
HZSM-5_40	195	0.326	400	0.249	0.574
Hβ1_12.5	195	0.586	370	0.371	0.957
Hβ2_12.5	190	0.412	350	0.378	0.790
HY_2.5	190	0.776	370	0.287	1.063
MCM-41_5	200	0.073	260	0.569	0.642
MCM-41_10	185	0.165	255	0.340	0.506
Co/HZSM-5_11.5	205	1.244	450	0.370	1.614
Cu/HZSM-5_11.5	205	0.899	440	0.875	1.774
Mn/HZSM-5_11.5	195	1.117	440	0.255	1.373

Above this group, the highest amount of acid sites is represented by the HZSM-5_11.5 catalyst (2.693 mmol NH_3/g_{cat}) followed by the HZSM-5_25 and HZSM-5_40 samples, showing values of 0.969 and 0.574 mmol NH_3/g_{cat}, respectively. These results indicate that the increment of Si/Al ratio reduces the amount of acid sites, which is in accordance with the results reported in literature [36,37]. In fact, the amount of chemisorbed NH_3 is closely related to the aluminum content in the catalysts, which plays an important role as acidity source in zeolites [38].

The profiles of the Hβs (Hβ1_12.5 and Hβ2_12.5) and HY_2.5 catalysts register another characteristic shape due to a contribution of two desorption peaks, being the most distinguishable the one that is linked to the weak-medium strength ones (around 190–195 °C) and the one related to strong acid sites in the range between 350 and 370 °C [26,34]. Therefore, the peak associated to strong acid sites of these catalysts is shifted at lower temperatures when compared with the HZSM-5 catalysts, indicating that the amount of strong acid sites in them is lower than in the HZSM-5 ones. The contribution of weak-medium acid sites, instead, is higher and, regarding total amount of acid sites considering these three catalysts, the one that shows the highest is the HY_2.5 zeolite, followed by the Hβ1_12.5 zeolite and, finally, the Hβ2_12.5 zeolite (see Table 2).

The ammonia desorption profiles of the MCM-41 catalysts represent the contribution of two peaks with similar shapes to those obtained in bibliography [37]. The maximum temperatures for each desorption peak are around 185–200 °C and 255–260 °C (see Table 2), suggesting that these catalysts hold, mainly, weak and medium acid sites [39]. Regarding the total amount of acid sites, the MCM-41_10 catalyst has the lowest acidity, since the MCM-41_5 catalyst shows a total acidity closer to the Hβ1_12.5 catalyst one.

Concerning to the monometallic catalysts, the incorporation of metal species on the HZSM-5_11.5 zeolite decreases the maximum temperature ascribed to weak-medium acid sites. In contrast, the maximum temperature attributed to strong acid sites remains almost constant. Nevertheless, the intensity of the peak related to the strong acid sites shows a drastic drop on every of the metal-containing catalysts profiles (see Fig. 3), meaning that the strength of those strong acid sites is affected by the metal incorporation. Therefore, the total acidity of these samples is mainly due to their weak-medium acid sites. The strong acid sites disappearance could also suggest that the incorporated metals are mainly deposited over these strong acid sites of the support, indicating that metal species have more affinity for strong acid sites and end blocking these ones.

3.1.3. Fourier-transform infrared spectroscopy

3.1.3.1. Py-FTIR. As aforementioned, the Py-FTIR was used to discriminate between the type of acid sites (Brønsted or Lewis) and to quantify the density of these acid sites among the different employed catalysts. The deconvolution of the obtained spectra provides peaks at different adsorption bands and quantitative data related to the ratio of Brønsted and Lewis acid sites (BAS/LAS), which are shown in Table 3. All these catalytic samples register characteristic bands at around 1545 and 1454 cm^{-1} bands (see Fig. 4 and Fig. 5), the first one associated with Brønsted acid sites (pyridinium ion) and the second one related with Lewis acid sites (pyridine coordinately bounded to accessible Al^{3+}) [40]. Between these two characteristic bands a third band appears, at 1490 cm^{-1}, this band is related to contribution of both type of acid sites, Lewis and Brønsted (and is not quantified in Table 3).

Above all the Py-FTIR characterized catalysts, the ones that provide the highest BAS/LAS ratio are the HZSM-5 ones, reaching their top value at 21.6 for the HZSM-5_11.5 catalyst. The integration value for the Brønsted peak is similar for the HZSM-5_25 and HZSM-5_40 catalysts, while the value corresponding to the Lewis peak decreases for the HZSM-5_40, providing for this catalyst higher BAS/LAS ratio than for the HZSM-5_25 catalyst.

In the case of the Hβ1_11.5 and Hβ2_11.5 catalysts, both β protonated zeolites, they show very similar BAS/LAS ratios due to the contribution of Brønsted and Lewis acidities, which are similar in both samples. The HY_2.5 catalyst shows slightly higher BAS/LAS ratio than the β protonated zeolites, because it has a greater contribution of Brønsted acid sites, while Lewis acid sites also increase but to a lesser extent.

The results showed in Table 3 indicate that, in general, Brønsted acidity contribution in the Hβ1_12.5, Hβ2_12.5 and HY_2.5 zeolites decreases when compared with HZSM-5 zeolites. This fact agrees with the NH_3-TPD profiles, where the peak detected at around 425–450 °C reduces its intensity and shifts to lower desorption temperatures when comparing the HZSM-5 catalysts to the other mentioned zeolites. In this sense, it seems probable that the NH_3 desorption peaks spotted at around 190–200 °C belong to Lewis acid sites, while peaks detected around 425–450 °C correspond to Brønsted acid sites [28,41].

Table 3
Py-FTIR numerical results.

Sample	BAS 1545 cm^{-1} $mmol \cdot g^{-1}$	LAS 1454 cm^{-1} $mmol \cdot g^{-1}$	BAS/LAS[a] $mmol \cdot mmol^{-1}$
HZSM-5_11.5	0.79	0.04	21.59
HZSM-5_25	0.20	0.08	2.41
HZSM-5_40	0.30	0.07	4.53
Hβ1_12.5	0.16	0.28	0.59
Hβ2_12.5	0.19	0.32	0.60
HY_2.5	0.23	0.31	0.75
Co/HZSM-5_11.5	0.25	0.77	0.32
Cu/HZSM-5_11.5	0.26	0.54	0.49
Mn/HZSM-5_11.5	0.33	0.57	0.57

[a] The applied molar extinction coefficients by Emeis [23].

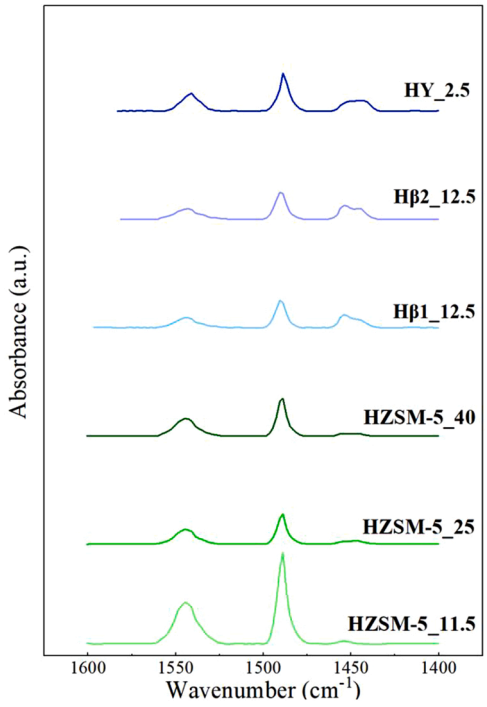

Fig. 4. Py-FTIR spectra of HZSM-5, Hβ and HY_2.5 zeolites.

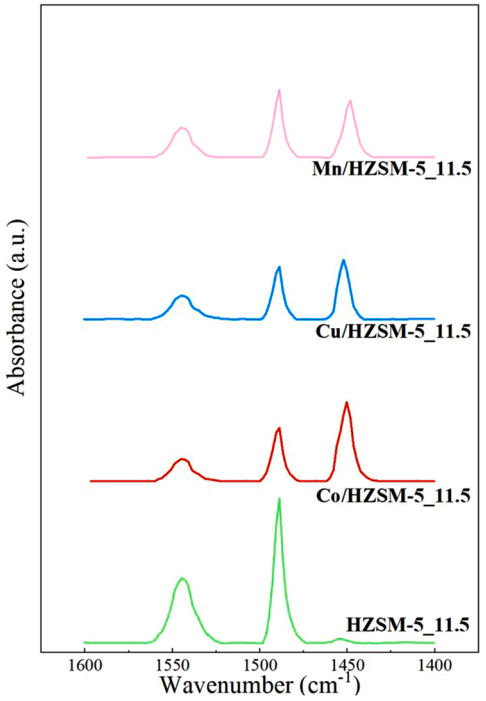

Fig. 5. Py-FTIR spectra of HZSM-5_11.5 catalyst and HZSM-5 with non-noble metals impregnated by wet-impregnation.

As shown in Fig. 5, the addition of metals by wet-impregnation on the HZSM-5_11.5 zeolite causes a drastic decrease of the Brønsted type acidity and a severely increase the Lewis acid sites. The reduction of BAS could be due to the preferential deposition of metals on BAS, which is in concordance with the NH_3-TPD results. As stated above, the LAS type acidity increases significantly, especially in the Co-loaded one, followed by the Mn and Cu ones.

3.1.3.2. CD_3CN-DRIFT. Deuterated acetonitrile (CD_3CN) was used as a complementary probe molecule to pyridine (Py) to evaluate the surface acidity of the samples. The use of CD_3CN allows to differentiate between Brønsted and Lewis acid sites, just like pyridine, but due to its higher sensitivity, this molecule also allows to distinguish the strength of the acid sites.

DRIFT spectra after CD_3CN adsorption are collected in Fig. 6. For the assignment of the infrared bands, it must be taken into account that the frequencies of the registered signals are $\geq$ 2300 cm^{-1} and are associated with Lewis acid sites, while that when they are $<$ 2300 cm^{-1} they are attributed to Brønsted acid sites. Furthermore, the strength of these acid centers increases with higher frequencies [42,43]. The intensity of all the spectra has been normalized with overtones of the Si-O bond.

Three infrared bands can be distinguished in the case of the HZSM-5 zeolites, except for the HZSM-5_11.5. These three peaks are associated with strong/medium Lewis acid sites ($L_{S/M}$) at 2318 cm^{-1}, strong Brønsted acid sites (B_S) at 2295 cm^{-1}, and weak Brønsted acid sites (B_W) at 2275 cm^{-1} [42,43]. Among the HZSM-5 supports, the HZSM-5_11.5 is the one that gives the highest signal for B_S and $L_{S/M}$, which means that this zeolite has the highest amount of both types of acid sites. Consequently, considering these results and those of Py-FTIR, the HZSM-5_11.5 is the catalyst with the highest BAS/LAS, and these BAS are also very strong.

The Hβs and HY_2.5 zeolites, also contained strong/medium Lewis acid sites, strong Brønsted acid sites and weak Brønsted acid sites, and most of their acidity splits between $L_{S/M}$ and B_W type of acid sites. Being well noted that the Hβ1_12.5 catalyst presents the highest value of strong/medium Lewis acid sites, unlike the HY_2.5 catalyst, whose highest peak is related to weak Brønsted acid sites.

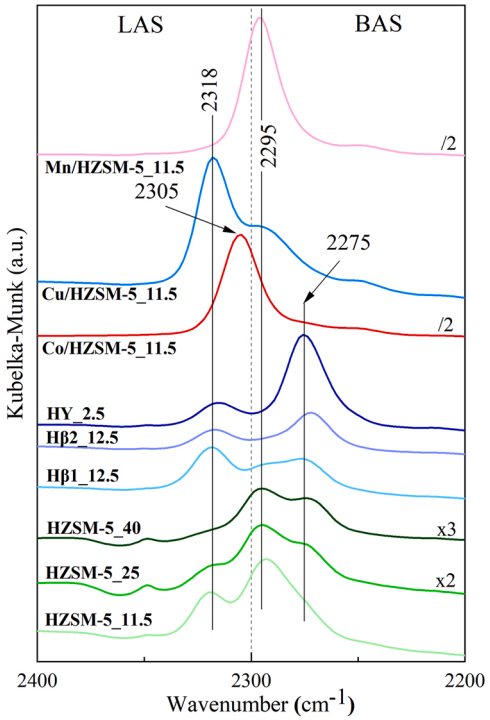

Fig. 6. DRIFT spectra for all of the employed catalysts.

The addition of non-noble metals on HZSM-5_11.5 significantly modified the nature and strength of the surface acid centers, as can be seen in Fig. 6 and Fig. 7 (deconvoluted spectra). With the addition of Co, a new peak appears at 2305 cm^{-1} that corresponds to Lewis weak acid sites (L_W) and it has been previously associated with the presence of Co^{2+} ions supported on zeolites [44–46]. In the Co/HZSM-5_11.5 catalyst, the peak related to medium/strong Lewis acid sites rises drastically compared to the parent zeolite in contrast to the strong Brønsted acid sites. The addition of Mn highly increases the peak related to strong Brønsted acid sites, but there is no presence of strong/medium Lewis acid sites, unlike weak Lewis acid sites. As aforementioned, the Mn/HZSM-5_11.5 has a low BAS/LAS ratio with higher presence of LAS so, combining these results, it could be said that, even though the presence of BAS is low, its strength is very high and the opposite is observed for LAS, its presence is higher but they have no or very little response peaks for interaction with CD_3CN. This difference could be due to the differences in pyridine and deuterated acetonitrile adsorptions [47,48].

MCM-41 catalysts were not analyzed by any of these FTIR methods due to the impossibility of compressing the sample, which is necessary to carry out the Py-FTIR analysis, and the small quantity available of each catalyst.

3.1.4. X-ray photoelectron spectroscopy

The XPS technique has been employed to get insights into the surface characteristics of the employed catalysts. Concretely, the XPS provided information about coordination state of the surface species and their ratio. The binding energies (BE) associated to O 1 s, Si 2p, Al 2p, Cu $2p_{3/2}$, CuLMM, Co $2p_{3/2}$, Mn $2p_{3/2}$ core levels are summarized in Table 4. As can be observed, all of the catalysts showed O 1 s, Si 2p and Al 2p peaks at around 533.4, 103.5 and 75 eV, which can be assigned to regular lattice oxygen from zeolites, Si^{+2} and Al^{+3} species [27,49,50], respectively. This fact indicated that O, Si and Al species coordination did not

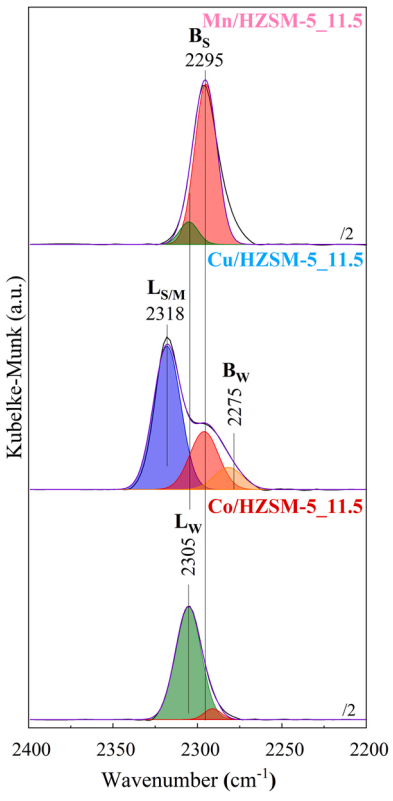

Fig. 7. Deconvolution results of DRIFT analysis of non-noble metal impregnated catalysts.

Table 4
Binding energies (eV), referenced to C1s= 284.8 eV, and surface Si/Al ratio.

Sample	O 1 s	Si 2p	Al 2p	Cu $2p_{3/2}$	CuLMM	Co $2p_{3/2}$	Mn $2p_{3/2}$	Ratio Si/Al
HZSM-5_11.5	533.4	103.7	74.9					11.3
HZSM-5_25	532.4	103.2	75.0					27.8
HZSM-5_40	533.1	103.6	74.8					42.5
Hβ1_12.5	533.1	103.8	74.9					15.5
Hβ2_12.5	532.9	103.6	75.2					12.0
HY_2.5	531.9	102.7	74.8					1.7
Co/HZSM-5_11.5	532.7	103.5	75.0			781.6		14.7
Cu/HZSM-5_11.5	532.5	103.2	74.9	933.5	573.6			11.4
Mn/HZSM-5_11.5	532.6	103.3	74.8				642.7; 646.7	12.5

*Note: Si/Al ratio follows the expected trend (seen in Table 1), being the values different because this is surface Si/Al ratio.

suffer variations. However, the detection of different values for O1s in the zeolites suggested de presence of different surface oxide species. Based on the literature [51] zeolites can be presented as Si-OH (533.7 eV), S═O (532.3 eV) and SiO_2 (533.1 eV) species on the surface.

Taking into account this and the data presented in Table 4, it seemed that the zeolites showed contribution of different species, being the silanol species more important for the HZSM-5_11.5 catalyst. This fact seemed to be in accordance with the high acidity presented by this catalyst. The binding energy of the O 1 s level for the other zeolites shifted to lower BEs suggesting a major contribution of other surface species such as S═O and SiO_2. The detection of these species could be due to the lower acidity presented by these zeolites when compared with HZSM-5_11.5.

Regarding metal catalysts, the Co supported zeolite presented a peak at 781.6 eV which corresponds to Co^{4+} species [52], fact that was confirmed by the presence of its satellite at 787.6 eV. The Cu/HZSM-5_11.5 catalyst showed Cu $2p_{3/2}$ level at 933.53 eV which can be ascribed to Cu^{+} [52,53]. The presence of this specie was also confirmed by the detection of CuLMM peak at 573.6 eV binding energy. The absence of the satellite peak in the Cu $2p_{2/3}$ level excluded the possibility of having Cu^{2+} species on the surface. Regarding the Mn/HZSM-5_11.5 catalyst, it showed two BE for Mn $2p_{3/2}$ peak, one at 642.7 and other at 646.7 eV, corresponding the first one to Mn^{2+} species and the second one could correspond to the MnO satellite feature [54]. According to the literature [55], the presence of the double peaks of Mn 2p implies that the Mn species are successfully introduced in the zeolite framework through interactions between Mn species and the silanols (Brønsted acid sites) to form Si-O-Mn.

Based on this, it seemed that Co, Cu and Mn addition reduced the Brønsted acid sites, as was confirmed by Py-FTIR measurements. On the other hand, the addition of metal species on HZSM-5_11.5 zeolite provoked a slight decrease on the binding energies ascribed to O 1 s level, reaching values close to 532.5 eV. This phenomenon could be related to the aforementioned phenomenon or to the presence of lattice oxygen from metal oxides. Apart from this, the Si/Al ratio slightly increases, which could indicate that the metal could be depositing on the surface of the Al.

3.2. Activity results

3.2.1. Preliminary tests for 1 and 3 h

The characterized acid catalysts were experimentally tested to study their catalytic activity at different reaction times, specifically at 1 and 3 h. The results are presented in Table 5 for the HZSM-5 type zeolites, Table 6 for the Hβs and HY_2.5 zeolites, and Table 7 for the MCM-41 catalysts.

Regarding HZSM-5 type catalysts, the catalytic activity for these zeolites after 1 h of reaction was similar. The increase of the reaction time from 1 h to 3 h improved the HMF conversion and yield towards MMF product, reaching values above 90 % and 75 %, respectively, for these catalysts. However, between these zeolites, the HZSM-5_40 showed better catalytic activity after 3 h of reaction than the HZSM-5_11.5 and HZSM-5_25 catalysts. In particular, this zeolite provided a complete HMF conversion and MMF yield of 95 %. The good behavior of this catalyst was followed by the HZSM-5_25 and HZSM-5_11.5 catalysts, respectively, which presented similar catalytic activity after 3 h of reaction.

Reaction mechanism of HMF reaction with methanol towards MMF could be extrapolated from the suggested one for the production of EMF with ethanol [17]. Being the reaction by-products, the 5-(dimethoxymethyl)− 2-furanmethanol (or 5-hydroxymethyl)− 2-(dimethoxymethyl)furan, HMFDMA), methyl levulinate (mL) and methyl formate (MF). Based on this, the enhancement of MMF yield, with little enhance of HMF conversion, when reaction time increases would be due to the transformation of HMFDMA into MMF. This by-product that equilibrates MMF generation has been identified by

Table 5
Catalytic activity results obtained with HZSM-5 catalysts. Reaction conditions: 160 °C, 20 bar of N_2, 500 rpm.

Sample	Reaction time h	HMF conversion %	MMF yield %
HZSM-5_11.5	1	89	74
	3	92	79
HZSM-5_25	1	90	74
	3	92	86
HZSM-5_40	1	92	76
	3	100	95

Table 6
Catalytic activity results for Hβ and HY catalysts. Reaction conditions: 160 °C, 20 bar of N_2, 500 rpm.

Sample	Reaction time h	HMF conversion %	MMF yield %
Hβ1_12.5	1	91	73
	3	92	33
Hβ2_12.5	1	94	86
	3	96	67
HY_2.5	1	36	25
	3	70	61

Table 7
Catalytic activity results for MCM-41 catalysts. Reaction conditions: 160 °C, 20 bar of N_2, 500 rpm.

Sample	Reaction time h	HMF conversion %	MMF yield %
MCM-41_5	1	65	59
	3	61	50
MCM-41_10	1	74	52
	3	94	69

GC/MS, together with mL, which can be obtained from MMF or HMF [17].

In the case of the Hβ1_12.5, Hβ2_12.5 and HY_2.5 zeolites, their catalytic activity showed more important differences than the HZSM-5 zeolites at the two different reaction times selected for preliminary tests. As can be observed in Table 6, the HMF conversion and the MMF yield for the Hβ1_12.5 and Hβ2_12.5 zeolites were similar to the obtained ones for the HZSM-5 after 1 h of reaction. The HY_2.5 zeolite presented a lower catalytic activity than its counterparts. Moreover, the increase in the reaction time enhanced HMF conversion, following the same trend as the one showed by the HZSM-5 catalysts. However, within the catalysts shown in Table 6, the HY_2.5 zeolite was the only catalyst that improved MMF yield when reaction time was increased. This mentioned catalyst provided an HMF conversion of 70 % and a yield towards MMF of 61 % at 3 h of reaction. Regarding the Hβ1_12.5 and Hβ2_12.5 catalysts, they enhanced the conversion of HMF until achieving its almost complete conversion, reaching values above 90 %. However, their ability to produce MMF decreased with the increment of reaction time from 1 h to 3 h. Specifically the Hβ1_12.5 catalyst provided a MMF yield of 73 % that decreased to 33 %. Although the Hβ2_12.5 catalyst presented the same trend regarding MMF yield as the Hβ1_12.5 catalyst, the decrease is less pronounced.

These phenomena, related to the enhancement of the HMF conversion and the decrease of the MMF yield, could suggest that MMF reacts under operation conditions. As previously mentioned, mL and MF could be formed from MMF, explaining the MMF yield decrease and the HMF conversion increase.

The important difference between the catalytic activity of the group of the HZSM-5 zeolites and the group of Hβ (Hβ1_12.5 and Hβ2_12.5) and HY_2.5 zeolites did not seem to be related with their textural properties. However, within these zeolites Hβs and HY_2.5, the textural properties also seem to play an important role when it adds up to the acidity. In contrast with Hβs, HY_2.5 zeolite possesses the smallest mesoporous volume, being its greater contribution of pore volume the microporous type one. This fact together with the presence of weak-medium acid strength and Brønsted acid sites, corroborated by NH_3-TPD and Py-FTIR, seems to be the responsible of the catalytic behavior presented by the HY_2.5 zeolite.

Total acidity, strength of acid sites, and ratio between Brønsted and Lewis acid sites of the catalysts seemed to play an important role in the HMF etherification reaction. In terms of acidity, the HZSM-5 catalysts exhibited stronger acid sites corroborated by maximum temperatures obtained by NH_3 desorption and FTIR analysis, using as probe molecules both pyridine and deuterated acetonitrile.

By the FTIR analysis, the majority of their acid sites were Brønsted acid sites, depicted by the high BAS/LAS ratio and, as previously seen in Fig. 4, these Brønsted acid sites are, above all, strong Brønsted acid sites. In this sense, the Hβ1_12.5, Hβ2_12.5, and HY_2.5 zeolites presented lower acid strength, having more Lewis type acid sites and weak type Brønsted acid sites when compared to the HZSM-5 catalysts. This observation suggests that a combination of acid strength (as measured by NH_3-TPD) and the greater presence of Brønsted acid sites (as estimated from Py-FTIR spectra), specifically strong Brønsted acid sites (as indicated by CD_3CN-FTIR), resulting in a higher BAS/LAS ratio, are key factors for HMF etherification, as reported literature proposes [56]. In this sense, the decrease in MMF yield with reaction time observed for the Hβ and HY catalysts could be a consequence of consecutive reactions of the MMF formed during the first hour caused by an increase in the Lewis acidity of these materials. These reactions, apart from the aforementioned by-products, could generate humins or heavy products, which can be accumulated in the active sites provoking the decrease of MMF yield, even the deactivation of the catalysts.

Regarding the MCM-41 catalysts, they showed different behaviors depending on the Si/Al ratio, as shown in Table 7. When Si/Al ratio is low, the catalyst provided a HMF conversion and a MMF yield below 65 % at 1 and 3 h. Moreover, in this case, these two activity parameters decreased when reaction time increased, indicating that this catalyst was not active toward HMF transformation and selective enough for MMF production after 1 h. The catalytic activity loss of MCM-41_5 catalyst could be due to the formation of humins [57] and, even, heavy products, generated from HMF degradation in water, that could lead the way to deactivate the catalysts.

As previously mentioned, this phenomenon was also observed for the Hβ1_12.5 and Hβ2_12.5 catalysts, being the loss of yield towards MMF for those two catalysts higher than the one detected for MCM-41 with low Si/Al ratio. On the other hand, the catalyst with higher Si/Al ratio presented higher HMF conversion at both reaction times and it improved the MMF yield from 52 % to 69 % when reaction time was increased. However, neither of these catalysts were able to provide similar HMF conversions and MMF yields when compared with the HZSM-5 catalysts. These two catalysts presented a similar total amount of acid sites than some of the other employed catalysts. Nevertheless, the maximum temperature of NH_3 desorption associated with the acid sites of this mentioned catalysts shifted from high temperatures (400 °C approx.) to low temperatures (260 °C approx.), indicating that the average strength of the MCM-41 s strong type acid sites is clearly lower than the strengths showed by the zeolites (HZSM-5 s, Hβs, and HY_2.5).

Among all the tested catalysts, the HZSM-5 s showed the best catalytic activity in the etherification reaction of HMF towards MMF, while the worst catalytic activity by means of MMF yield variation while increasing the reaction time, was for the Hβ1_12.5 zeolite. The good catalytic behavior of HZSM-5 zeolites could be referred to the higher acid strength of its acid sites and to the presence of more and stronger Brønsted acid sites. Considering these statements and the small difference observed in catalytic activity of the HZSM-5 catalysts, the next step was incrementing the reaction time up to 5 and 10 h.

3.2.2. *Activity test at higher reaction time for 5 and 10 h*

Results achieved under these conditions were collected in Table 8, where results of the HZSM-5 zeolites and the Hβ1_12.5 were presented for comparing them, as this was the catalyst (between Hβs and HY_2.5 catalysts) that seemed to have the worst performance through time. Also, in Fig. 8, results of the HZSM-5_11.5 and the Hβ1_12.5 are represented in order to see the tendency of the activity tests results using these two catalysts. Results of the Hβ1_12.5 showed that although longer reaction times increased the HMF conversion (at 5 and 10 h), it was not capable of improving the MMF yield, indicating that this catalyst is not selective enough towards the MMF formation. In this sense, this zeolite contained sites with similar acid strength than the ones of some HZSM-5 catalysts, providing similar HMF conversions. But it had higher strong/medium Lewis acid sites and low Brønsted ones, being these Brønsted

Table 8
Catalytic activity results with HZSM-5 catalysts and Hβ1_12.5 catalyst. Reaction conditions: 160 °C, 20 bar of N_2, 500 rpm.

Sample	Reaction time h	HMF conversion %	MMF yield %
HZSM-5_11.5	1	89	74
	3	92	79
	5	98	97
	10	98	68
HZSM-5_25	1	90	74
	3	92	86
	5	96	90
	10	96	65
HZSM-5_40	1	92	76
	3	100	95
	5	100	85
	10	100	63
Hβ1_12.5	1	91	73
	3	92	33
	5	96	22
	10	98	12

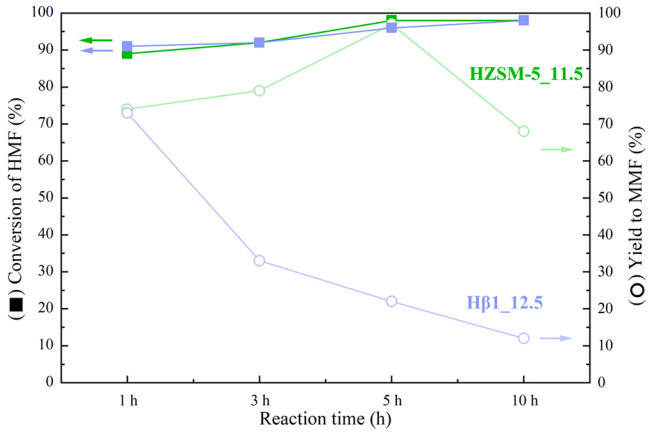

Fig. 8. Catalytic activity results with HZSM-5_11.5 (in green) and Hβ1_12.5 (in blue) through reaction time. Filled squares are for conversion of HMF and empty circles for yield to MMF.

acid sites distributed between strong and weak. These facts seem to be the cause of the decrease in the BAS/LAS ratio, provoking the lower MMF yields obtained.

Regarding HZSM-5 catalysts, the HMF conversion remained constant between 3 and 10 h of reaction time when the HZSM-5_40 catalyst was used, while the MMF yield was reduced from 95 % to 63 %. The HZSM-5_11.5 and HZSM-5_25 zeolites enhanced the HMF conversion and the MMF yield up until 5 h of reaction time. However, after 10 h of reaction, the HMF conversion remained almost constant while the MMF yield decreased from 97 % to 68 % using the HZSM-5_11.5 catalyst, and from 90 % to 65 % using the HZSM-5_25 one. In this sense, and as can be seen in Table 8, all the HZSM-5 catalysts showed a severe decrease in the MMF yield when 10 h of reaction time were reached. Based on these catalytic results, the catalyst that showed the best performance along time was the HZSM-5_11.5, showing its best performance after 5 h of reaction time, achieving values around 97 % for the MMF yield and 98 % for the HMF conversion. In contrast, HZSM-5_40, achieved its highest at 3 h but its stability decreased by increasing reaction time, probably due to deactivation of these catalyst through reaction time.

Within the HZSM-5 catalysts, the one that showed a drastically higher amount of acid sites is the HZSM-5_11.5 zeolite, being the strength and type of them mostly strong Lewis and, above all, strong Brønsted acid sites. These were the reasons that led to conclude that this type of acid centers is the one that most favors the reaction, resulting in better selectivity results towards MMF production.

In summary, based on the results, it can be seen that the best behavior is presented by HZSM-5_11.5 and HZSM-5_40 zeolites. In the case of HZSM-5_40, a yield of 95 % towards MMF is reached earlier, however, by increasing reaction time, this catalyst loses selectivity towards the product desired in this study, reaching a yield of 63 % at 10 h. In the case of the HZSM-5_11.5, the yield is slightly higher after 5 h of reaction time, being its selectivity towards the MMF practically complete. However, after 5 h it also loses selectivity although this loss is slightly lower than in the case of HZSM-5_40. The good performance of the HZSM-5_11.5 can be associated to its acid characteristics, such as high acid strength, high concentration of acid sites, specifically, Brønsted acid sites and, consequently, high BAS/LAS ratio.

Based on these observations, the HZSM-5_11.5 zeolite was employed as support of different non-noble metals, specifically: Co, Cu and Mn, being the metal content of around 3 wt%. These prepared metal catalysts were tested at the same reaction conditions as the bare zeolites, choosing as reaction time 5 h, trying to see if the incorporation of these metal affects in the HZSM-5_11.5 performance. The activity results achieved with these metal containing catalysts are displayed in Table 9. As can be observed, the incorporation of different metals did not improve the catalytic activity of the HZSM-5_11.5 support. In particular, the presence of Co and Cu in the zeolite reduced the catalytic activity of the bare support, resulting in a lower HMF conversion and a lower MMF yield. The presence of Mn seemed to have no influence on the activity of the HZSM-5_11.5 support, based on the HMF conversions and MMF yields, which were almost the same as the ones obtained with the bare support.

Table 9
Catalytic activity results, 5 h reaction time, with HZSM-5_11.5 catalyst and HZSM-5_11.5 with non-noble metals. Reaction conditions: 160 °C, 20 bar of N_2, 500 rpm.

Sample	HMF conversion %	MMF yield %
HZSM-5_11.5	98	97
Co/HZSM-5_11.5	88	85
Cu/HZSM-5_11.5	94	87
Mn/HZSM-5_11.5	98	97

The behavior of these metal catalysts can again be related to the loss of part of their acid sites (see Table 2) due to the preferential disposition of metals over Brønsted type acid sites in the case of Cu and Co incorporation, which has been confirmed as the most interesting type of acid site to favor the reaction towards the desired product, the MMF. On the contrary, in the case of Mn incorporation, although the BAS/LAS ratio (Py-FTIR) decreases, the presence of strong Brønsted acid sites (CD_3CN-DRIFT) maintains the initial performance of the HZSM-5_11.5 zeolite. Therefore, it is not only important to have a high BAS/LAS ratio, but also strong Brønsted acid sites are required to reach high HMF conversions and MMF yields.

Regarding repeatability catalytic tests for the HZSM-5_11.5 zeolite were performed in triplicate, obtaining an experimental error around ± 6 %.

4. Conclusions

The catalytic conversion of HMF through its etherification towards MMF was carried out in a discontinuous batch type reactor, employing as catalysts different silico-alumina catalysts (most of them with zeolitic structure). The most promising zeolite type catalyst was the selected one to be used as support of newly prepared catalysts by non-noble metal (Co, Cu, and Mn) wet-impregnation.

All the catalysts were tested for the desired reaction, maintaining constant all the operation conditions with the exception of the reaction time. Starting with reaction times of 1 and 3 h, all catalysts were tested and MCM-41 catalysts were discarded for further experiments, as well as the HY_2.5 zeolite and the Hβ2_12.5 zeolite because of their poorer behavior; keeping for the next step the HZSM-5 zeolites as well as the Hβ1_12.5 zeolite.

The activity results were analyzed taking into account the information from the characterization of the catalysts. The results of these characterization techniques confirmed that acidity was the most important catalyst characteristic to explain the differences in activity and selectivity observed for the different catalytic samples. Confirming that the HZSM-5_11.5 and the HZSM-5_40 zeolites are the ones that present greater behavior in the production of MMF having, both, higher concentration of BAS than LAS. However, Lewis and Brønsted acid sites could be active in the HMF etherification, but strong Brønsted acid sites, as seen in HZSM-5_11.5 catalyst, were the most selective for the formation of the MMF as product.

The addition of non-noble metals to the HZSM-5_11.5 zeolite did not lead to any improvement, seeming that the addition of metal blocked part of the strong acid centers of this catalyst. The incorporation of metal did not change the structure of the HZSM-5_11.5 but, in general, decreased significantly the BAS/LAS ratio.

CRediT authorship contribution statement

P. Díaz-Maizkurrena: Conceptualization, Methodology, Validation, Investigation, Resources, Writing – original draft, Writing – review & editing, Visualization. **J. Requies:** Conceptualization, Methodology, Validation, Writing – review & editing, Supervision, Project administration, Funding acquisition. **A. Iriondo:** Conceptualization, Methodology, Validation, Writing – original draft, Writing – review & editing, Visualization, Supervision, Project administration. **R. Mariscal:** Investigation. **P.L. Arias** : Writing - review.

Declaration of Competing Interest

The authors declare that they have no known competing financial interests or personal relationships that could have appeared to influence the work reported in this paper.

Data availability

Data will be made available on request.

Acknowledgements

This research was supported by the University of the Basque Country (UPV/EHU), Basque Government (IT1554-22), and the Spanish Ministry of Economy, Industry and Competitiveness (PID2021-122736OB-C43 and PID2021-122736OB-C41). The authors express their gratitude to Roberto Palos and Iratxe Crespo from the Chemical Engineering department of the UPV/EHU for their help and assistance, for letting us use their FTIR equipment. The authors also express their gratitude to Pedro J. Maireles from the Inorganic Chemistry, Crystallography and Mineralogy department of the University of Málaga (UMA) for performing all XPS analyses.

References

[1] B. Oberle, S. Bringezu, S. Hatfield-Dodds, S. Hellweg, H. Schandl, J. Clement, Global Resources Outlook 2019: Natural Resources for the Future We Want, Nairobi, Kenya, 2020. https://doi.org/10.18356/689a1a17-en.

[2] S. Bringezu, A. Ramaswami, H. Schandl, M. O'Brien, R. Pelton, J. Acquatella, E.T. Ayuk, A. Shun Fung Chiu, R. Flanegin, J. Fry, S. Giljum, S. Hashimoto, S. Hellweg, K. Hosking, Y. Hu, M. Lenzen, M. Lieber, S. Lutter, A. Miatto, A. Singh Nagpure, M. Obersteiner, L. van Oers, S. Pfister, P.-P. Pchler, A. Russell, L. Spini, H. Tanikawa, E. van der Voet, H. Weisz, J. West, A. Wiijkman, B. Zhu, R. Zivy, Assessing Global Resource Use: a Systems Approach to Resource Efficiency and Pollution Reduction, Nairobi, Kenya, 2017. ⟨https://www.resourcepanel.org/reports/assessing-global-resource-use⟩.

[3] J.C. Serrano-Ruiz, J.A. Dumesic, Catalytic routes for the conversion of biomass into liquid hydrocarbon transportation fuels, Energy Environ. Sci. 4 (2011) 83–99, https://doi.org/10.1039/C0EE00436G.

[4] L. Bernstein, P. Bosch, O. Canziani, Z. Chen, R. Christ, O. Davidson, W. Hare, S. Huq, D. Karoly, V. Kattsov, Z. Kundzewicz, J. Liu, U. Lohmann, M. Manning, T. Matsuno, B. Menne, B. Metz, M. Mirza, N. Nicholls, L. Nurse, R. Pachauri, J. Palutikof, M. Parry, D. Qin, N. Ravindranath, A. Reisinger, J. Ren, K. Riahi, C. Rosenzweig, M. Rusticucci, S. Schneider, Y. Sokona, S. Solomon, P. Stott, R. Stouffer, T. Sugiyama, R. Swart, D. Tirpak, C. Vogel, G. Yohe, Climate Change 2007: the Physical Science Basis: Contribution of Working Group I to the Fourth Assessment Report of the Intergovernmental Panel on Climate Change, Cambridge University Press, Geneva, Switzerland, 2007. ⟨https://www.ipcc.ch/report/ar4/wg1/⟩.

[5] European Commission, The European Green Deal, in: Brussels, 2019, 24. ⟨https://eur-lex.europa.eu/legal-content/EN/TXT/HTML/?uri=CELEX:52019DC0640&from=EN⟩.

[6] E. Baldoni, G. Philippidis, J. Spekreijse, P. Gurría, T. Lammens, C. Parisi, T. Ronzon, M. Vis, R. M'Barek, Getting your hands dirty: a data digging exercise to unearth the EU's bio-based chemical sector, Renew. Sustain. Energy Rev. 143 (2021), 110895, https://doi.org/10.1016/j.rser.2021.110895.

[7] European Commission, Chemicals Strategy for Sustainability Towards a Toxic-Free Environment, in: Brussels, 2020, 24. ⟨https://eur-lex.europa.eu/legal-content/EN/TXT/HTML/?uri=CELEX:52020DC0667&from=EN⟩.

[8] D. Zhao, T. Su, Y. Wang, R.S. Varma, C. Len, Recent advances in catalytic oxidation of 5-hydroxymethylfurfural, Mol. Catal. 495 (2020), 111133, https://doi.org/10.1016/j.mcat.2020.111133.

[9] S.J. Howard, K.A. Kreutzer, B. Rajagopalan, E.R. Sacia, A. Sanborn, B. Smith, Processes for Producing 2,5-Furandicarboxylic Acid and Derivatives Thereof and Polymers Made therefrom, US 2018/0093961 A1, 2018. ⟨https://patents.google.com/patent/US20180093961A1/en⟩.

[10] J. Lewkowski, Synthesis, chemistry and applications of 5-hydroxymethyl-furfural and its derivatives, ARKIVOC 2001 (2001) 17–54, https://doi.org/10.3998/ark.5550190.0002.102.

[11] S.P. Teong, G. Yi, Y. Zhang, Hydroxymethylfurfural production from bioresources: past, present and future, Green Chem. 16 (2014) 2015, https://doi.org/10.1039/c3gc42018c.

[12] J.J. Bozell, G.R. Petersen, Technology development for the production of biobased products from biorefinery carbohydrates—the US Department of Energy's "Top 10" revisited, Green Chem. 12 (2010) 539, https://doi.org/10.1039/b922014c.

[13] N. Viar, J.M. Requies, I. Agirre, A. Iriondo, M. Gil-Calvo, P.L. Arias, Ni–Cu bimetallic catalytic system for producing 5-hydroxymethylfurfural-derived value-added biofuels, ACS Sustain. Chem. Eng. 8 (2020) 11183–11193, https://doi.org/10.1021/acssuschemeng.0c02433.

[14] C. Muñoz de Diego, W.P. Schammel, M.A. Dam, G.J.M. Gruter, Method for the Preparation of 2,5-furandicarboxylic Acid and Esters Thereof, WO 2011/043660 A2, 2011. ⟨https://patentscope.wipo.int/search/en/detail.jsf?docId=WO2011043660⟩.

[15] E. Mazoyer, A.S. Vagueiro de Sousa Dias, B. McKay, H.J. Baars, V.P.C. Vreeken, G. J.M. Gruter, D.L. Sikkenga, Process for the Preparation of 2,5-Furan-dicarboxylic Acid, US 9,643, 945 B2, 2017. ⟨https://patents.google.com/patent/US9643945/fr⟩.

[16] A. Serrano, J. Carro, A.T. Martínez, Reaction mechanisms and applications of aryl-alcohol oxidase, in: in: The Enzymes, Elsevier, 2020, pp. 167–192, https://doi.org/10.1016/bs.enz.2020.05.005.

[17] S. Alipour, H. Omidvarborna, D.-S. Kim, A review on synthesis of alkoxymethyl furfural, a biofuel candidate, Renew. Sustain. Energy Rev. 71 (2017) 908–926, https://doi.org/10.1016/j.rser.2016.12.118.

[18] G. Lin, W. Lin, J. Wu, Y. Zhan, F. Okejiri, M. Weng, J. Fu, Oxidation of 5–methoxymethylfurfural to 2, 5-furandicarboxylic acid over Ru/hydroxyapatite catalyst in water, Chem. Eng. Sci. 249 (2022), 117343, https://doi.org/10.1016/j.ces.2021.117343.

[19] J. Carro, E. Fernández-Fueyo, C. Fernández-Alonso, J. Cañada, R. Ullrich, M. Hofrichter, M. Alcalde, P. Ferreira, A.T. Martínez, Self-sustained enzymatic cascade for the production of 2,5-furandicarboxylic acid from 5-methoxymethylfurfural, Biotechnol. Biofuels 11 (2018), 86, https://doi.org/10.1186/s13068-018-1091-2.

[20] L. Hu, L. Lin, Z. Wu, S. Zhou, S. Liu, Recent advances in catalytic transformation of biomass-derived 5-hydroxymethylfurfural into the innovative fuels and chemicals, Renew. Sustain. Energy Rev. 74 (2017) 230–257, https://doi.org/10.1016/j.rser.2017.02.042.

[21] G.J.M. Gruter, F. Dautzenberg, Method for the Synthesis of 5-hydroxymethylfurfural Ethers and Their Use, US 2011/0082304 A1, 2011. ⟨https://patentimages.storage.googleapis.com/22/b4/df/647b1729eeb8f1/US20110082304A1.pdf⟩.

[22] S. Vichaphund, D. Aht-ong, V. Sricharoenchaikul, D. Atong, Production of aromatic compounds from catalytic fast pyrolysis of Jatropha residues using metal/HZSM-5 prepared by ion-exchange and impregnation methods, Renew. Energy 79 (2015) 28–37, https://doi.org/10.1016/j.renene.2014.10.013.

[23] C.A. Emeis, Determination of integrated molar extinction coefficients for infrared absorption bands of pyridine adsorbed on solid acid catalysts, J. Catal. 141 (1993) 347–354.

[24] J. Wei, T. Wang, X. Cao, H. Liu, X. Tang, Y. Sun, X. Zeng, T. Lei, S. Liu, L. Lin, A flexible Cu-based catalyst system for the transformation of fructose to furanyl ethers as potential bio-fuels, Appl. Catal. B Environ. 258 (2019), 117793, https://doi.org/10.1016/j.apcatb.2019.117793.

[25] Q. Yao, Y. Liu, D. Zhang, M. Sun, X. Ma, Catalytic conversion of a $\geq$ 200 °C fraction separated from low-temperature coal tar into light aromatic hydrocarbons, ACS Omega 6 (2021) 4062–4073, https://doi.org/10.1021/acsomega.0c06123.

[26] F. Jokar, S.M. Alavi, M. Rezaei, Investigating the hydroisomerization of n-pentane using Pt supported on ZSM-5, desilicated ZSM-5, and modified ZSM-5/MCM-41, Fuel 324 (2022), 124511, https://doi.org/10.1016/j.fuel.2022.124511.

[27] A. Iriondo, J.F. Cambra, V.L. Barrio, M.B. Guemez, P.L. Arias, M.C. Sanchez-Sanchez, R.M. Navarro, J.L.G. Fierro, Glycerol liquid phase conversion over monometallic and bimetallic catalysts: effect of metal, support type and reaction temperatures, Appl. Catal. B Environ. 106 (2011) 83–93, https://doi.org/10.1016/j.apcatb.2011.05.009.

[28] T.C. Hoff, D.W. Gardner, R. Thilakaratne, K. Wang, T.W. Hansen, R.C. Brown, J.-P. Tessonnier, Tailoring ZSM-5 zeolites for the fast pyrolysis of biomass to aromatic hydrocarbons, ChemSusChem 9 (2016) 1473–1482, https://doi.org/10.1002/cssc.201600186.

[29] F. Lónyi, J. Valyon, On the interpretation of the NH3-TPD patterns of H-ZSM-5 and H-mordenite, Microporous Mesoporous Mater. 47 (2001) 293–301, https://doi.org/10.1016/S1387-1811(01)00389-4.

[30] M. Rutkowska, I. Pacia, S. Basąg, A. Kowalczyk, Z. Piwowarska, M. Duda, K. A. Tarach, K. Góra-Marek, M. Michalik, U. Díaz, L. Chmielarz, Catalytic performance of commercial Cu-ZSM-5 zeolite modified by desilication in NH 3 -SCR and NH 3 -SCO processes, Microporous Mesoporous Mater. 246 (2017) 193–206, https://doi.org/10.1016/j.micromeso.2017.03.017.

[31] J. Li, S. Ma, R. Cui, N. Xu, T. Pei, NO oxidation with H2O2 catalyzed by zeolites in a fixed-bed reactor: experimental and mechanism, Mol. Catal. 528 (2022), 112494, https://doi.org/10.1016/j.mcat.2022.112494.

[32] T. Chen, C. Gu, Y. Ouyang, L. Zhuang, Z. Yao, K. Zou, Y. Wang, Y. Luo, X. Shu, Synthesis of high hydrothermal stability Beta zeolite with crosslinked starch and catalytic performance in catalytic cracking reaction, Fuel 318 (2022), 123696, https://doi.org/10.1016/j.fuel.2022.123696.

[33] K.B. Golubev, O.V. Yashina, N.N. Ezhova, N.N. Kolesnichenko, Gas-phase oxidative carbonylation of methane to acetic acid over zeolites, Mendeleev Commun. 31 (2021) 712–714, https://doi.org/10.1016/j.mencom.2021.09.040.
[34] A. Sultana, T. Nanba, M. Sasaki, M. Haneda, K. Suzuki, H. Hamada, Selective catalytic reduction of NOx with NH3 over different copper exchanged zeolites in the presence of decane, Catal. Today 164 (2011) 495–499, https://doi.org/10.1016/j.cattod.2010.11.036.
[35] H. Li, L. Sheng, J. Zhan, W. Fang, Y. Liang, Y. Zhang, Comparative study on the catalytic performance of zeolite catalysts with different topologies in 1-methylnaphthalene isomerization-transalkylation coupling reaction, J. Fuel Chem. Technol. 49 (2021) 809–817, https://doi.org/10.1016/s1872-5813(21)60035-x.
[36] A.M. Camiloti, S.L. Jahn, N.D. Velasco, L.F. Moura, D. Cardoso, Acidity of Beta zeolite determined by TPD of ammonia and ethylbenzene disproportionation, Appl. Catal. A Gen. 182 (1999) 107–113, https://doi.org/10.1016/S0926-860X(98)00418-9.
[37] A.M. Venezia, R. Murania, V. La Parola, B. Pawelec, J.L.G. Fierro, Post-synthesis alumination of MCM-41: effect of the acidity on the HDS activity of supported Pd catalysts, Appl. Catal. A Gen. 383 (2010) 211–216, https://doi.org/10.1016/j.apcata.2010.06.001.
[38] M. Marosz, B. Samojeden, A. Kowalczyk, M. Rutkowska, M. Motak, U. Díaz, A. E. Palomares, L. Chmielarz, MCM-22, MCM-36, and ITQ-2 zeolites with different Si/Al molar ratios as effective catalysts of methanol and ethanol dehydration, Materials 13 (2020) 2399, https://doi.org/10.3390/ma13102399.
[39] L. Alvarado-Perea, J.A. Colín-Luna, A. López-Gaona, T. Wolff, J.G. Pacheco-Sosa, J. C. García-Martínez, Simultaneous adsorption of quinoline and dibenzothiophene over Ni-based mesoporous materials at different Si/Al ratio, Catal. Today 353 (2020) 26–38, https://doi.org/10.1016/j.cattod.2019.11.025.
[40] F. Benaliouche, Y. Boucheffa, P. Ayrault, S. Mignard, P. Magnoux, NH3-TPD and FTIR spectroscopy of pyridine adsorption studies for characterization of Ag- and Cu-exchanged X zeolites, Microporous Mesoporous Mater. 111 (2008) 80–88, https://doi.org/10.1016/j.micromeso.2007.07.006.
[41] S.A. Bates, W.N. Delgass, F.H. Ribeiro, J.T. Miller, R. Gounder, Methods for NH3 titration of Brønsted acid sites in Cu-zeolites that catalyze the selective catalytic reduction of NOx with NH3, J. Catal. 312 (2014) 26–36, https://doi.org/10.1016/j.jcat.2013.12.020.
[42] A.G. Pelmenschikov, R.A. van Santen, J. Janchen, E. Meijer, CD3CN as a probe of lewis and bronsted acidity of zeolites, J. Phys. Chem. 97 (1993) 11071–11074, https://doi.org/10.1021/j100144a028.
[43] M. Muñoz-Olasagasti, I. Martínez-Salazar, M.L. Granados, C. López-Aguado, J. Iglesias, G. Morales, R. Mariscal, Elucidating the roles of acid site nature and strength in the direct conversion of levulinic acid into ethyl valerate: the case of Zr-modified beta zeolite-supported Pd catalysts, Sustain. Energy Fuels 6 (2022) 1164–1174, https://doi.org/10.1039/D1SE01802G.
[44] M. Muñoz-Olasagasti, M. López Granados, C.P. Jiménez-Gómez, J.A. Cecilia, P. Maireles-Torres, J.A. Dumesic, R. Mariscal, The relevance of Lewis acid sites on the gas phase reaction of levulinic acid into ethyl valerate using CoSBA-xAl bifunctional catalysts, Catal. Sci. Technol. 11 (2021) 4280–4293, https://doi.org/10.1039/d1cy00166c.
[45] J. Chen, J.M. Thomas, G. Sankar, IR spectroscopic study of CD3CN adsorbed on ALPO-18 molecular sieve and the solid acid catalysts SAPO-18 and MeAPO-18, Faraday Trans. 90 (1994) 3455, https://doi.org/10.1039/ft9949003455.
[46] O. Bortnovsky, Z. Sobal, Exchange of Co(II) ions in H-BEA zeolites: identification of aluminum pairs in the zeolite framework, Microporous Mesoporous Mater. 46 (2001) 265–275, https://doi.org/10.1016/S1387-1811(01)00307-9.
[47] Y. Akacem, E. Kassab, Vibrational analysis of pyridine adsorption on the Brønsted acid sites of zeolites based on density functional cluster calculations, J. Phys. Chem. C 112 (2008) 19045–19054, https://doi.org/10.1021/jp8069354.
[48] C. Morterra, M. Peñarroya Mentruit, G. Cerrato, Acetonitrile adsorption as an IR spectroscopic probe for surface acidity/basicity of pure and modified zirconias, Phys. Chem. Chem. Phys. 4 (2002) 676–687, https://doi.org/10.1039/b109047j.
[49] S. Bawaked, K. Narasimharao, Structural and catalytic properties of copper silicate nanomaterials, Sci. Rep. 10 (2020), 518, https://doi.org/10.1038/s41598-020-57502-z.
[50] C. Liu, R. Kang, F. Bin, X. Wei, K.N. Hui, S. Kasipandi, K.S. Hui, Insights on copper, manganese, and Nickel/ZSM-5 catalytic mechanisms for nitric oxides selective reduction with ammonia, Carbon Resour. Convers. 5 (2022) 15–25, https://doi.org/10.1016/j.crcon.2021.11.002.
[51] X. Xing, X. Shi, M. Ruan, Q. Wei, Y. Guan, H. Gao, S. Xu, Sulfonic acid functionalized β zeolite as efficient bifunctional solid acid catalysts for the synthesis of 5-hydroxymethylfurfural from cellulose, Int. J. Biol. Macromol. (2023), 125037, https://doi.org/10.1016/j.ijbiomac.2023.125037.
[52] NIST X-ray Photoelectron Spectroscopy Database, Version 4.1, National Institute Standards and Technology, Gaithersburg, (2012). ⟨https://doi.org/10.18434/T4T88K⟩.
[53] I. Platzman, R. Brener, H. Haick, R. Tannenbaum, Oxidation of polycrystalline copper thin films at ambient conditions, J. Phys. Chem. C 112 (2008) 1101–1108, https://doi.org/10.1021/jp076981k.
[54] A. Ghods, C. Zhou, I.T. Ferguson, Structural and optical properties of (Zn,Mn)O thin films prepared by atomic layer deposition, J. Vac. Sci. Technol. A 38 (2020), 042408, https://doi.org/10.1116/6.0000141.
[55] Y. Zeng, Q. Zhuo, L. Dai, B. Guan, Mn anchored zeolite molecular nest for enhanced catalytic ozonation of cephalexin, Chemosphere 335 (2023), 139058, https://doi.org/10.1016/j.chemosphere.2023.139058.
[56] M. Zuo, W. Jia, Y. Feng, X. Zeng, X. Tang, Y. Sun, L. Lin, Effective selectivity conversion of glucose to furan chemicals in the aqueous deep eutectic solvent, Renew. Energy 164 (2021) 23–33, https://doi.org/10.1016/j.renene.2020.09.019.
[57] L. Bing, Z. Zhang, K. Deng, Efficient one-pot synthesis of 5-(ethoxymethyl)furfural from fructose catalyzed by a novel solid catalyst, Ind. Eng. Chem. Res. 51 (2012) 15331–15336, https://doi.org/10.1021/ie3020445.